Heliyon 10 (2024) e35263

Contents lists available at ScienceDirect

Heliyon

journal homepage: www.cell.com/heliyon

Research article

Screening chondrocyte necroptosis-related genes in the diagnosis and treatment of osteoarthritis

Muhai Deng [a], Cong Tang [a], Li Yin [b], Junjun Yang [c], Zhiyu Chen [d,e], Yunsheng Jiang [a], Yang Huang [f,**], Cheng Chen [a,*]

[a] College of Medical Informatics, Chongqing Medical University, Chongqing, 400016, China
[b] Department of Orthopaedics, General Hospital of Western Theater Command, Chengdu, 610083, China
[c] Key Laboratory of Biorheological Science and Technology, Ministry of Education College of Bioengineering, Chongqing University, Chongqing, 400044, China
[d] Orthopedic Laboratory of Chongqing Medical University, Chongqing, 400016, China
[e] Department of Orthopedics, The First Affiliated Hospital of Chongqing Medical University, Chongqing, 400016, China
[f] State Key Laboratory of Trauma, Burns and Combined Injury, Department of Wound Infection and Drug, Daping Hospital, Army Medical University, Chongqing, 400042, China

ARTICLE INFO

Keywords:
Osteoarthritis
Chondrocytes
Necroptosis
Machine learning

ABSTRACT

Background: Osteoarthritis (OA) is the most common form of joint diseases, with hallmark of cartilage degeneration. Recent studies have shown that the pathogenesis of OA is associated with chondrocyte necroptosis.

Methods: In this study, we used single-cell RNA sequencing (scRNA-seq) and bulk RNA sequencing data to analyze necroptosis regulation in OA chondrocytes. We performed enrichment analysis, carried out experimental validation, constructed machine learning models, and docked drug molecules.

Results: After least absolute shrinkage and selection operator (LASSO) algorithm screening, 4 hub genes (RIPK3, CYBB, HSP90AB1, and TRAF5) with diagnostic characteristics were obtained. Following the comparison of multiple models, the Bayesian model with an average area under curve (AUC) value of 0.944 was finally selected. We found that nimesulide exhibited strong binding affinity to CYBB and HSP90AB1, and experimentally verified that nimesulide reduced the expression of RIPK3 and CYBB, suggesting its potential as an inhibitor of chondrocyte necroptosis. Furthermore, scRNA-seq results showed that necroptosis in OA was significantly upregulated on regulatory chondrocytes (RegC) compared to other chondrocyte subtypes.

Conclusions: The results indicate that nimesulide might be used to treat OA by inhibiting chondrocyte necroptosis through down-regulation of RIK3 and CYBB genes. This study reveals the role of chondrocyte necroptosis in OA, and suggests a potential therapeutic strategy by regulating necroptosis with nimesulide.

* Corresponding author.
** Corresponding author.
E-mail addresses: huangyang@tmmu.edu.cn (Y. Huang), ccllljff@163.com (C. Chen).

https://doi.org/10.1016/j.heliyon.2024.e35263
Received 24 April 2024; Received in revised form 18 July 2024; Accepted 25 July 2024
Available online 31 July 2024

1. Introduction

Osteoarthritis (OA), the most common form of joint diseases, is primarily characterized by disrupted articular cartilage homeostasis with following inflammation and degradation [1,2]. Articular cartilage is an avascular tissue containing almost only cell type, chondrocytes [3]. The death of chondrocytes, including autophagy [4,5], pyroptosis [6], apoptosis [7–9], and necroptosis [10,11], is involved in OA progression.

Necroptosis is a programmed form of necrosis [12]. The core event in necroptosis is the formation of the detergent-insoluble "necrosome" complex of homologous Ser/Thr kinases receptor interacting kinase 1 (RIPK1) and receptor interacting kinase 3 (RIPK3), which promotes phosphorylation of a key pro-death effector mixed lineage kinase domain-like (MLKL) by RIPK3. In OA, the activation of RIPK1- bone morphogenetic protein 7 (BMP7) functional axis has been shown to promote chondrocyte necroptosis [10]; similarly, perturbation of the TRIpartite motif-containing protein 24 (TRIM24) -RIPK3 axis also accelerates OA pathogenesis by activating RIPK3 and regulating the expression of catabolic factors [11]. These studies indicate that chondrocyte necroptosis is closely related to OA progression. Therefore, it is necessary to further study the intrinsic relationship between chondrocyte necroptosis and OA. At the same time, with the rapid advancement of sequencing technology, researchers have investigated the biochemical processes and pathogenesis of OA at the single-cell level. Ji et al. identified 7 chondrocyte subtypes within 1464 chondrocytes and explored the gene expression profiles of each subtype, elucidating their roles in the early treatment and diagnosis of OA [13]. Moreover, a study using single-cell RNA sequencing (scRNA-seq) identified a chondrocyte subtype characterized by the preferential expression of ferroptosis-related features and genes [14]. However, the use of scRNA-seq data in necroptosis-related research on OA remains limited.

In this study, firstly we screened necroptosis-related differentially expressed genes (DEGs) based on bulk RNA-seq data. Secondly, we constructed an OA diagnostic model, identified drugs capable of regulating chondrocyte necroptosis, and verified the analysis results through cellular experiments. Finally, through scRNA-seq data analysis, we explored the specificity of necroptosis in chondrocyte subtypes and investigated the communication between different chondrocyte subtypes. In conclusion, our work provides a comprehensive understanding of the mechanisms of necroptosis in OA at both bulk RNA-seq and scRNA-seq levels, and identifies key genes regulating necroptosis in OA cartilage.

2. Materials and methods

2.1. Data source

We downloaded datasets from Gene Expression Omnibus (GEO) (https://www.ncbi.nlm.nih.gov/geo) and BioStudies (www.ebi.ac.uk/biostudies). The gene expression profiling dataset GSE114007 [15] included 18 controls and 20 OA cartilage tissues of the human knee joint. Datasets GSE98918 [16], GSE129147 [17], and ERP105501 [18] as validation sets included 12 OA and 12 controls, 10 OA and 9 controls, and 65 OA and 7 controls, respectively. We used scRNA-seq data from GSE169454 dataset [19], including 3 control samples and 4 OA samples. Additionally, necroptosis-related genes were searched in Kyoto Encyclopedia of Genes and Genomes (KEGG) pathway database, and 159 genes were found. All data used in this study are available through previous publications or public domain.

2.2. Necroptosis related DEGs identification

Surrogate variable analysis ("sva" package in R) was used to correct batch effect arising from different platforms. The effectiveness of correction was assessed using Principal Component Analysis (PCA). We screened the DEGs between OA patients and control individuals in GSE114007 using "Deseq" package. The following criteria were statistically significant: adj.P.Val <0.05 and $|\log2FC| > 0.5$. Finally, necroptosis-related DEGs were obtained by intersecting DEGs with the above necroptosis-related genes.

2.3. Functional enrichment analysis and PPI network

Using adjusted $P < 0.05$ as threshold, we performed Gene Ontology (GO) and KEGG enrichment analysis. The relevant protein association as a protein-protein interaction (PPI) network was next constructed using the Search Tool for the Retrieval of Interacting Genes (STRING) database (www.string-db.org) [20].

2.4. Weighted gene co-expression network analysis

We used the weighted gene co-expression network analysis (WGCNA) to identify co-expressed genes in GSE114007 dataset. Pearson correlation coefficient was used to calculate the distance, and a weighted gene co-expression network was constructed by the "WGCNA" R package. The soft threshold was 6, and the module was then identified. After that, we set 50 as the minimum number for each gene module. $|MM|$ ($|$Module membership$|$) > 0.3 and $|GS|$ ($|$gene significance$|$) > 0.4 were defined as the screening criteria for filtering key genes in the candidate module.

2.5. Immune infiltration of DEGs related to necroptosis

We used single-sample gene set enrichment analysis (ssGSEA) to evaluate the scores of different immune cells and necroptosis using

"GSVA" package. The relationship between immune cells and necroptosis scores was analyzed by this function. The correlations between modules and immune cells were also calculated using "WGCNA" package. We utilized the "venn" package to identify overlaps among DEGs, key module genes, and necroptosis genes.

2.6. Identification of hub genes and development of prediction model

To choose linear models and keep the diagnostic hub genes, the "glmnet" package was used to perform the least absolute shrinkage and selection operator (LASSO) regression. The regularization parameter was determined through 10-fold cross-validation, and the final model selected the optimal lambda value that minimized the cross-validation error. Utilizing gene data refined through LASSO, we employed the "mlr3vers" R package for benchmark testing. We built 7 machine learning models using the lrn function from the "mlr3vers" package and identified the best model based on several model evaluation metrics. To ascertain the model's predictive accuracy, we further subjected it to validation using external datasets GSE98918, GSE129147, and ERP105501.

2.7. Molecular docking and molecular dynamics simulation

We validated the potential disease-related compounds in Toxicogenomics Database (CTD) (http://ctdbase.org/) [21] and PubChem database (https://pubchem.ncbi.nlm.nih.gov/) [22]. AutoDock 4.2.6 and the MM/PBSA. py module were used to calculate the free binding energy. PyMOL 2.5.0 (https://pymol.org/2/) was used for visualization. A 100 ns Molecular Dynamics (MD) simulation of the complex was performed using Gromacs 2023. The protein was modeled with CHARMM 36 force field parameters, while the ligand topology was constructed using GAFF2 force field parameters [23]. Periodic boundary conditions were applied, placing the protein-ligand complex in a cubic box. The box was filled with water molecules using the TIP3P water model, and sodium and chloride ions were added to neutralize the system and maintain physiological ionic strength. Electrostatic interactions were handled using Particle Mesh Ewald (PME) and the Verlet algorithm. The heavy atoms of the protein were constrained, and energy minimization was performed for 50000 steps using the steepest descent method. The simulation system was equilibrated for 100 ps using the NVT and NPT ensembles. Van der Waals and Coulomb interactions were calculated with a cutoff of 1.0 nm. Finally, a 100 ns molecular dynamics simulation was conducted at constant temperature (300 K) and pressure (1 bar) with a time step of 2 fs, and trajectory data were saved every 10 ps.

2.8. Real-time quantitative polymerase chain reaction (RT-qPCR) and Western blot

To create an in vitro OA model, we treated ATDC5 cells (Fenghui Biology, Hunan, China) with 10 ng/mL of IL-1β (Abbkine, Wuhan, China) for 24 h. For the drug group, 3 μg/mL of nimesulide (MCE, Shanghai, China) was added for another 24 h. Then, we collected cells from control group, IL-1β group, and nimesulide treatment group. RT-qPCR was performed using SYBR Green Premix Pro Taq HS qPCR Kit (Accurate Biology, Hunan, China) with a reaction volume of 20 μL. Each sample was tested in triplicate. The primers were listed in Table 1.

To further confirm the expression of the above genes at protein level, we performed Western blot. The following antibodies were used: ACAN (Affintiy, Jiangsu, China), MMP13 (Abcam, Boston, USA), RIPK3 (ZEN-BIOSCIENCE, Chengdu, China), CYBB (ZEN-BIOSCIENCE, Chengdu, China), HSP90AB1 (ZEN-BIOSCIENCE, Chengdu, China), TRAF5 (Boster, Wuhan, China), and β-actin (ZEN-BIOSCIENCE, Chengdu, China). After washing three times with TBST, the membranes were then incubated with HRP-conjugated secondary antibodies (Affintiy, Jiangsu, China) for 1 h at room temperature. Protein bands were visualized using the ECL Western Blotting Detection System (Vilber, Paris, France), and quantified using Image Lab 3.0 software (Bio-Rad, CA, USA). All experiments were performed in triplicate.

2.9. Immunofluorescence

The ADTC5 cells were washed with PBS and then fixed with 4 % paraformaldehyde. After fixation, the cells were blocked with Quick Blocking Buffer. Next, the cells were incubated with primary antibodies against CYBB (ZEN-BIOSCIENCE), HSP90AB1 (ZEN-BIOSCIENCE), TRAF5 (Boster), and RIPK3 (ZEN-BIOSCIENCE), each at a working concentration of 1:100. This was followed by incubation with a secondary antibody, Goat Anti-Rabbit IgG H&L (Alexa Fluor® 488), at a working concentration of 1:200. Nuclei were stained with DAPI. Fluorescence images were observed using a laser scanning confocal microscope, and the relative fluorescence

Table 1
The primers used for RT-qPCR in this study.

Gene Symbol	Forward	Reverse
β-actin	AGATCAAGATCATTGCTCCTCCT	ACGCAGCTCAGTAACAGTCC
ACAN	AAGAGATGGAGGGTGAGGTCTTT	CGTGCAGATAGACAGTCCTTACA
MMP13	GCTATTCTGGCCACCTTCTTCTT	GCCAGYCACAYCYAAGCCAAAGA
RIPK3	GACCTCAAGCCCTCTAACATTCT	AGCTGTAGACATCACTCGCTTTA
HSP90AB1	TCGGATTCTACTCGGCCTATCTA	TGCGAATGTTTCTTCACCACTTC
CYBB	TGCCAACTTCCTCAGCTACAATA	GTGTTCACTTGCAATGGTCTTGA
TRAF5	GCTGAGCAAGACTGTCCCTTTAA	GATCCGCTGTTCTAGTTGGTAGT

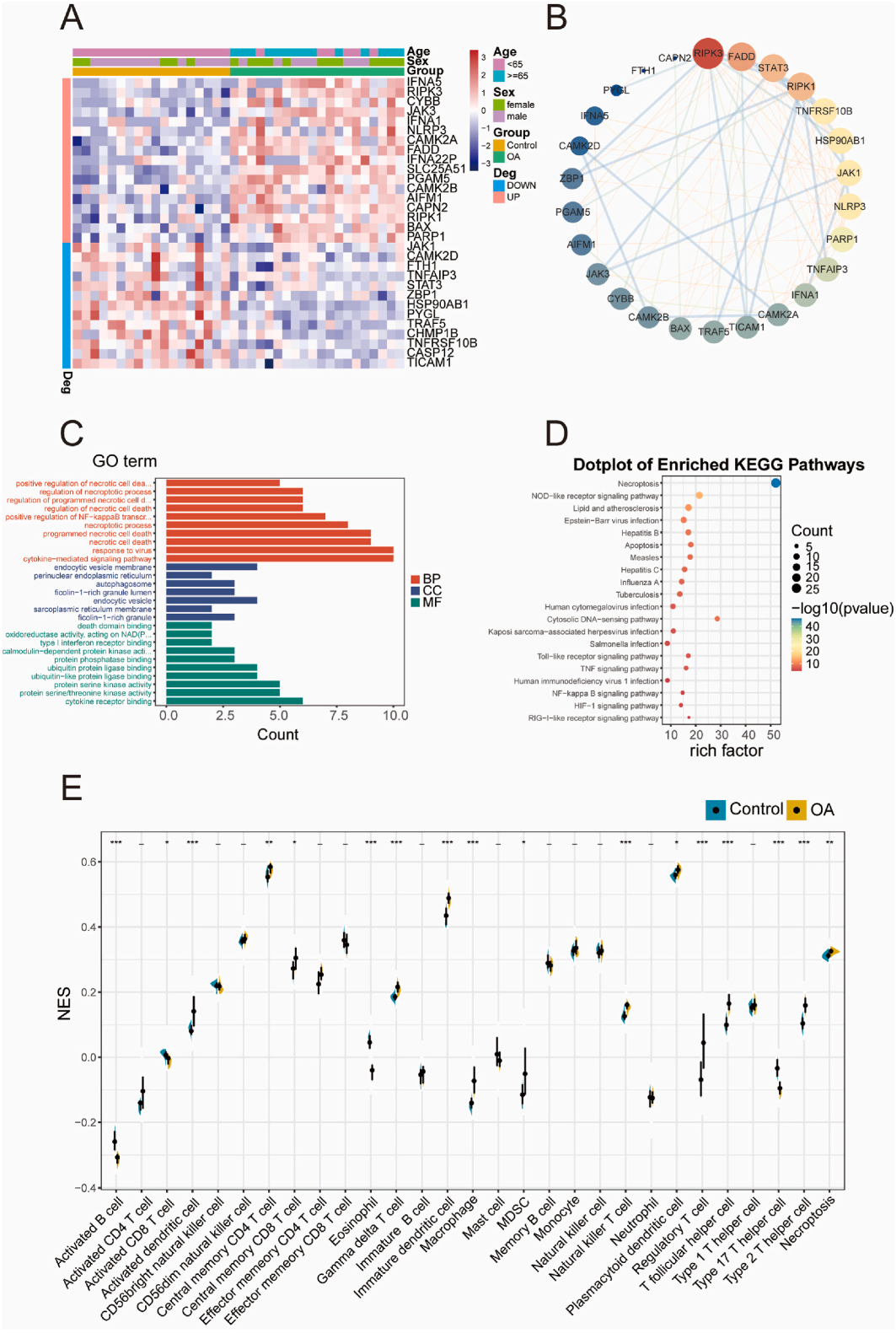

Fig. 1. Functional enrichment of necroptosis-related DEGs and immune infiltration. **A** Heatmap displaying the expressions of the 30 DEGs related to necroptosis. **B** PPI network of DEGs related to necroptosis based on STRING. **C** GO analysis of DEGs related to necroptosis. **D** KEGG analysis of DEGs related to necroptosis. **E** Immunocyte infiltration (*p < 0.05, **p < 0.01, ***p < 0.001).

intensity was analyzed with ImageJ (version 1.52p).

2.10. Visualization of OA sample cell types

We processed the scRNA-seq matrix by Seurat function. nFeature_RNA >500 & nFeature_RNA <4000, percent_mt < 5, nCount_RNA <20000 set as filtration threshold. Uniform Manifold Approximation and Projection (UMAP) and T-Stochastic Neighbor Embedding (t-SNE) function were used for visualizing cell populations. Referring to previous reports, we did the cell annotation. The marker genes were shown as following. Homeostatic chondrocytes (HomC): *JUN*, *MMP3*, and *FOSB*; prehypertrophic chondrocytes (preHTC): *COL10A1*, *IBSP*, *COL2A1*, and *TGFBI*; hypertrophic chondrocytes (HTC): *COL10A1*, *IBSP*, and *JUN*; regulatory chondrocytes (RegC): *CHI3L1* and *CHI3L2*; fibrochondrocytes (FC): *COL1A1*, *COL1A2*, *S100A4*, *PRG4*, and *TMSB4X*; reparative chondrocytes (RepC): *COL2A1*, *CILP*, *COL3A1*, and *COMP*; prefibrocartilage chondrocytes (preFC): *IL11*, *COL2A1*, *CILP*, and *OGN*; effector chondrocytes (EC): *TF*, *CHRDL2*, and *KIF9* [13,24,25].

2.11. Phenotype scoring of necroptosis

The phenotype scores of necroptosis were determined using the AddModuleScore algorithm of R package “Seurat”. Then, based on the median phenotype scores, the OA and control samples were divided into high- and low-necroptosis groups, followed by GSEA and KEGG analysis.

2.12. Cell-cell communication analysis

To explore the interactions among various cell types, we used “CellChat” package for cell communication analysis. Adhering to the official workflow, we examined the communication between cells in control and OA groups. We imported normalized counts from “Seurat” into “CellChat” and executed standard preprocessing procedures. The identification of ligand-receptor pairs involved evaluating the likelihood of interaction and conducting perturbation tests. We then constructed cell-cell communication networks by merging the significant ligand-receptor pairs and their associated degrees. To ascertain changes in signaling pathways due to cartilage injury, we compared the information flow within these pathways between control and OA cartilage tissues. Additionally, we computed the Euclidean distance between each pair of shared signaling pathways.

2.13. Statistical analysis

The Student’s t-test or the Wilcoxon rank-sum test was used to detect significant differences between two independent groups. The Kruskal-Wallis test was employed to explore differences among more than two independent groups. Unless otherwise stated, a p value less than 0.05 was considered statistically significant.

3. Results

3.1. Identification of necroptosis in OA

After batch effect removal (Figs. S1a and b), we normalized the data (Fig. S1c). We first recognized 4448 DEGs in GSE114007 dataset, of which 2412 genes were highly expressed, and 2036 genes were lowly expressed in OA. 159 necroptosis-related genes were obtained, and they were crossed with DEGs. Finally, a total of 30 DEGs related to necroptosis (17 up-regulated and 13 down-regulated) were identified. Hierarchical clustering heatmaps were used to display the expression patterns of these genes, alongside relevant clinical data (Fig. 1A). The PPI network showed that RIPK1 and FADD were with higher numbers of interacted proteins (Fig. 1B).

3.2. Enrichment analysis and WGCNA analysis

The GO analysis results revealed that these genes were mostly enriched in positive regulation of necrotic cell death, regulation of necroptotic process, and regulation of programmed necrotic cell death for biology process (BP); endocytic vesicle membrane, endocytic vesicle, and ficolin-1-rich granule lumen for cellular components (CC); cytokine receptor binding, protein serine/threonine kinase activity, and type I interferon receptor binding for molecular function (MF) (Fig. 1C). The KEGG analysis (Fig. 1D) results showed that the top 5 terms were Necroptosis, Cytosolic DNA-sensing pathway, NOD-like receptor signaling pathway, Apoptosis-multiple species, and Apoptosis. The WGCNA results showed the scale-free topological model fitting index (R2) reached 0.81 (Fig. S1d). After that, a total of 21 modules were identified in the dataset (Fig. S1e). Each module contained different gene clusters, and the correlation between modules was shown in Fig. S2a.

3.3. Immune characteristics in OA

Our results showed that Type 2 T helper cell, Natural killer T cell, and Macrophage had higher infiltration in OA samples than in control samples, and necroptosis scores also showed the similar trend (Fig. 1E). Next, we calculated the correlation among modules, OA traits, immune cells, and necroptosis. The results showed that the green module had the strongest positive correlation with OA

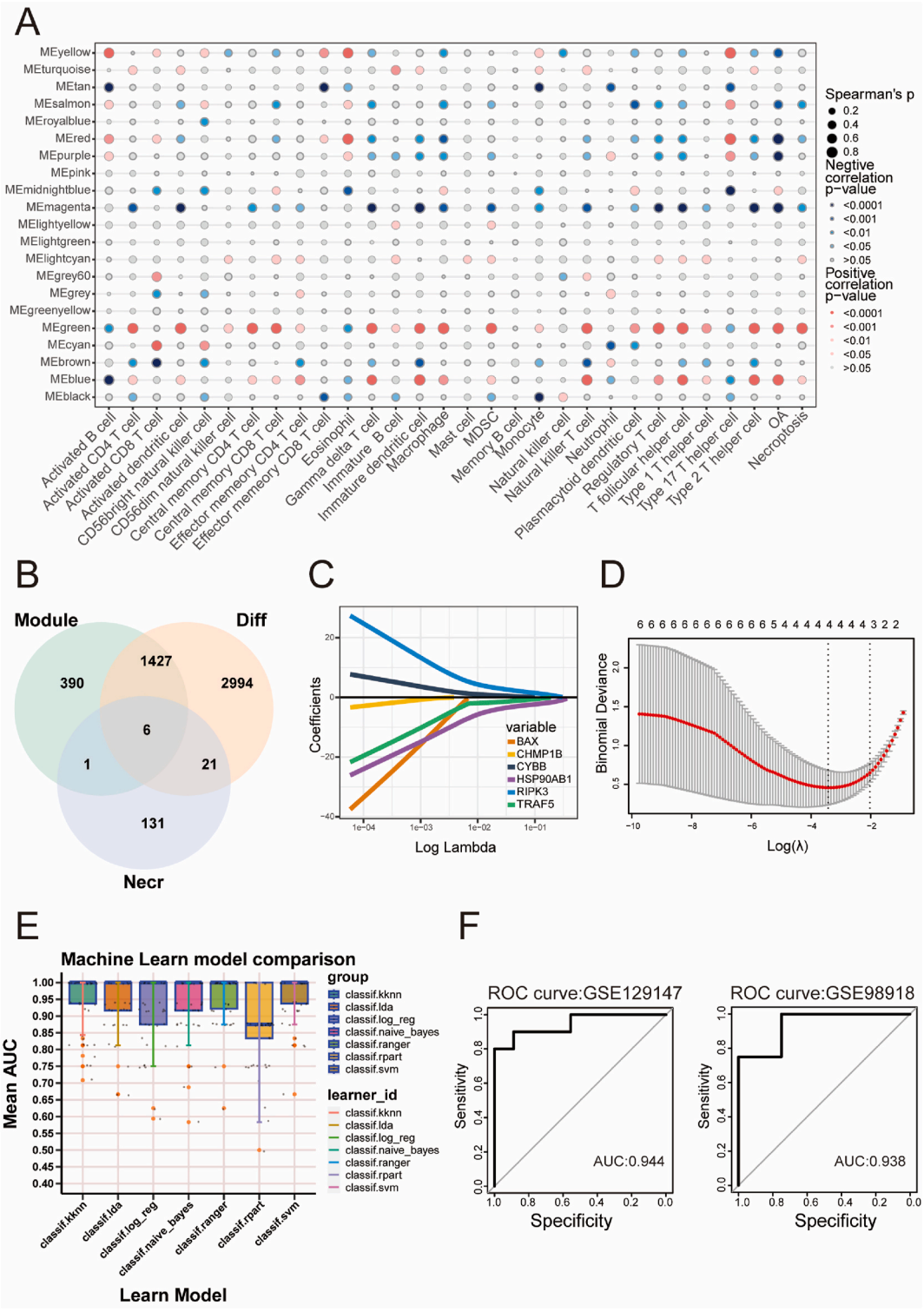

Fig. 2. Screening and identifying hub genes associated with necroptosis. **A** Module-trait relationships between WGCNA modules and immune cells. **B** Venn diagrams of the DEGs, genes of key modules, and necroptosis genes. **C, D** Feature selection by LASSO regression model in train dataset of GSE114007. **E** AUC comparison of multiple machine learning models. **F** ROC curves for the external data validation set GSE129147, GSE98918.

traits (0.76) and the red module exhibited the strongest negative correlation (−0.88). Moreover, the green module also had a positive correlation with macrophages (0.81), while the red module had a negative correlation with macrophages (−0.53) in Fig. 2A. Gene-module and gene-trait correlations were determined, and hub genes were identified using thresholds of $|GS| > 0.4$ and $|MM| > 0.3$. The colored parts in the upper right corners of Fig. S2b, c were the hub genes of the two modules. Finally, we identified 6 DEGs related to necroptosis and immunity (CHMP1B, HSP90AB1, TRAF5, BAX, CYBB, and RIPK3), as shown in Fig. 2B.

3.4. Genetic diagnostic model construction and validation

We conducted LASSO logistic regression analysis using 6 DEGs related to necroptosis and immunity. Fig. 2C presented the calculated regression coefficient, and Fig. 2D showed the tenfold cross-validation for tuning parameter selection in the LASSO regression. Eventually, we obtained 4 hub genes (RIPK3, CYBB, HSP90AB1, and TRAF5). Subsequently, based on the 4 hub genes, we did receiver operating characteristic (ROC) curves and boxplots in GSE114007 dataset for further validation (Figs. S2d and e). GSE129147 dataset also showed the similar results (Figs. S2f and g). Similarly, depending on 4 hub genes, we constructed 7 machine learning models on the GSE114007 dataset and obtained the corresponding area under curve (AUC) values, which represent the predictive accuracy of the models (Fig. 2E). Finally, we found that the Bayesian model showed the better false positive rate and specificity. Based on this model, we calculated the risk scores. As shown in Fig. 2F and Fig. S2h, the risk scores had a favorable diagnostic ability for OA discrimination. The AUC of the external validation datasets GSE129147, GSE98918, and ERP105501 was 0.944, 0.938, and 0.878, respectively.

3.5. Correlation of immune infiltration to hub genes

The CYBB and RIPK3 showed a strong correlation with the infiltration of 28 types of immune cells, a more pronounced correlation than observed with HSP90AB1 and TRAF5 (Fig. 3A). Among immune cells, regulatory T cells, macrophages, and T follicle helper cells exhibited a strong correlation with the RIPK3, CYBB, and HSP90AB1 genes. Notably, macrophages demonstrated a correlation and high reliability with these 3 hub genes (RIPK3, CYBB, and HSP90AB1). Among them, CYBB has the highest correlation, reaching 0.83, compared to RIPK3 and HSP90AB1, as illustrated in Fig. 3B. To assess the validity of our correlation analysis, we utilized the ERP105501 dataset for verification and drew congruent conclusions (Fig. 3C).

3.6. Molecular drug-docking and MD simulation

To explore prospective small molecule drugs for the treatment of OA, we utilized the CTD databases for chemical interactions and diseases data related to CYBB, RIPK3, HSP90AB1, and TRAF5 (Supplementary Tables 1, 2, 3, and 4). Although no suitable drugs were found in the results for RIPK3 and TRAF5, nimesulide was identified as effectively regulating both HSP90AB1 and CYBB in drug screening results. To further illustrate the effects of nimesulide on HSP90AB1 and CYBB, we conducted molecular docking experiments. Interactions between compounds and targets exhibited the highest free binding energy scores along with their binding modes in Fig. 3D and E. The results calculated using Autodock indicate that the binding energies of CYBB (3A1F) and HSP90AB1 (5UC4) are −5.92 kcal/mol and −4.92 kcal/mol, respectively. To quantitatively assess the binding energies further, we used the MM/PBSA method to compute the binding free energies of the complexes. The binding energies for HSP90AB1 (5UC4) and CYBB (3A1F) were found to be −44.390 kJ/mol and −49.215 kJ/mol, respectively. Negative values indicate binding affinity between the molecules and the target proteins, with lower values representing stronger binding forces. Therefore, this suggests that both CYBB and HSP90AB1 have good binding affinities with nimesulide.

To ensure thorough sampling of the conformational space, we performed 100 ns MD simulations for each protein-ligand complex. The results showed that CYBB (3A1F) with the nimesulide exhibited a smaller RMSD and better conformational stability compared to HSP90AB1 (5UC4) (Fig. 3F). Additionally, the Rg values for CYBB (3A1F) with the nimesulide showed more stable fluctuations, indicating that the CYBB (3A1F) protein remained stably compact throughout the simulation (Fig. 3G). The solvent accessible surface area (SASA) also indicated that there was no significant expansion or contraction of CYBB (3A1F) and HSP90AB1 (5UC4) proteins upon binding with the ligand nimesulide (Fig. S2i). Finally, by comparing the Root-mean-square-fuctuation (RMSF) results, we found that most amino acid residues in CYBB (3A1F) exhibited lower RMSF values, suggesting that the ligand can inhibit protein flexibility, thereby affecting protein function (Fig. S2j). In contrast, HSP90AB1 (5UC4) showed higher overall RMSF fluctuations when bound to the ligand, indicating greater flexibility (Fig. S2k).

3.7. Validation of hub genes expression and interaction with nimesulide

To validate our findings, we first conducted immunofluorescent staining on ADTC5 cells. The results showed that after IL-1β stimulation, the fluorescent intensities of the 4 hub genes (CYBB, HSP90AB1, RIPK3, and TRAF5) were all increased, with CYBB and RIPK3 aligning with our analysis trends (Fig. 4A). Additionally, to verify the molecular docking results, we further conducted qRT-PCR and WB experiments. In the qRT-PCR results, MMP13, RIPK3, CYBB, TRAF5, and HSP90AB1 had a significant rise in IL-1β group compared to control group, but these genes showed down-regulation after adding nimesulide (Fig. 4B). This implied that nimesulide might alleviate OA progression by affecting necroptosis-related genes. In the WB results, compared with control group, we found that the expression of RIPK3 and CYBB in IL-1β group was significantly increased. After nimesulide treatment, a decrease in RIPK3 and CYBB levels was observed (Fig. 4C and D). Meanwhile, with the addition of IL-1β, the expression of MMP13 was increased and the

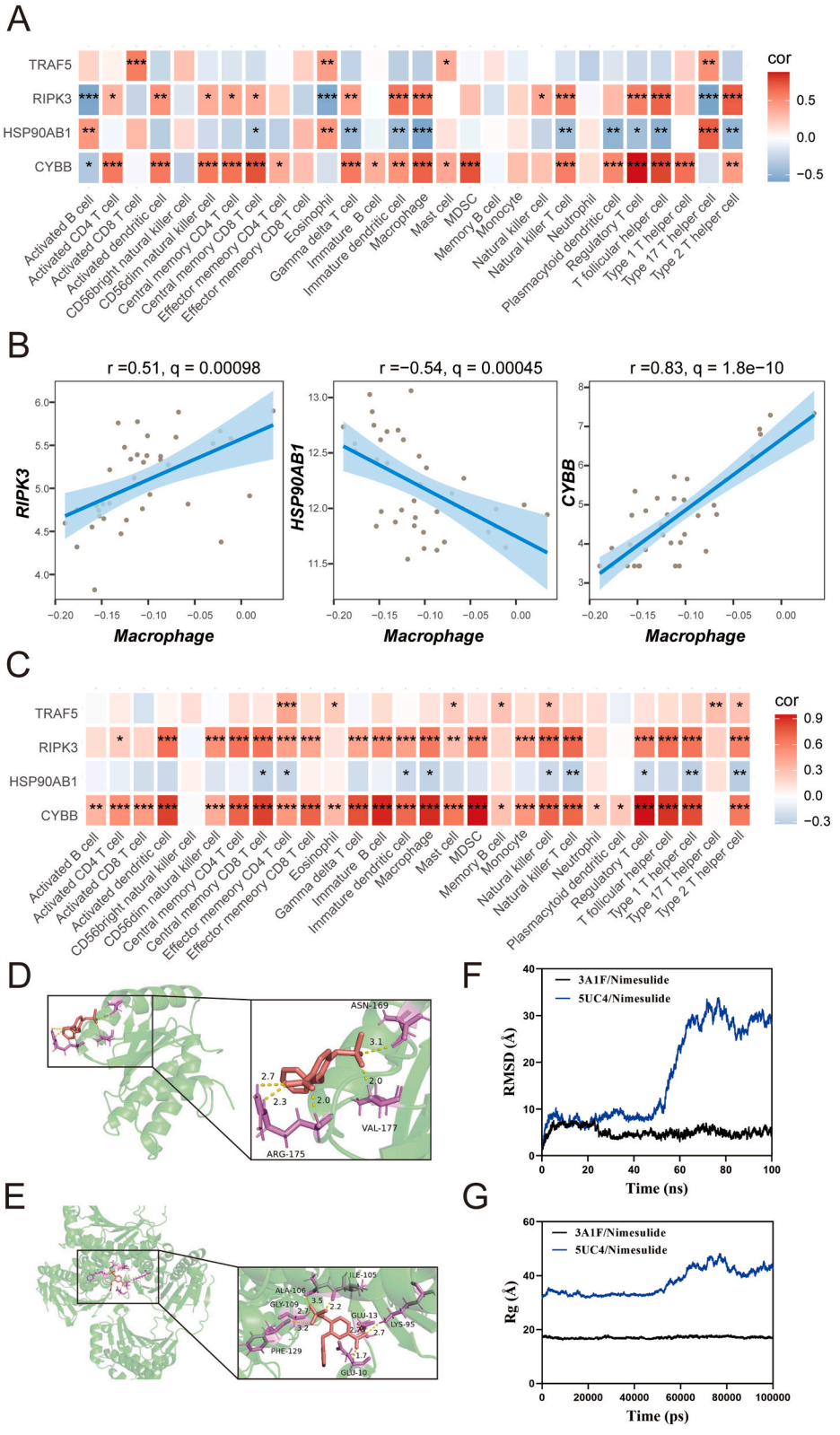

(caption on next page)

Fig. 3. Immune cell correlation analysis, molecular docking, and MD simulations of 4 hub genes. **A** Heatmaps showing the associations among 4 hub genes and immune cells in GSE114007. **B** Macrophage correlation analysis with RIPK3, HSP90AB1, and CYBB. **C** The associations among 4 hub genes and immune cells in ERP105501. **D** Nimesulide molecularly docked with CYBB (PDB: 3A1F). **E** Nimesulide molecularly docked with HSP90AB1 (PDB: 5UC4). **F** The Root-mean-square deviation (RMSD) graph for the CYBB (PDB: 3A1F) and the HSP90AB1 (PDB: 5UC4) with the ligand nimesulide. **G** The Radius of Gyration (Rg) graph for CYBB (PDB: 3A1F) and HSP90AB1 (PDB: 5UC4) with the ligand nimesulide.

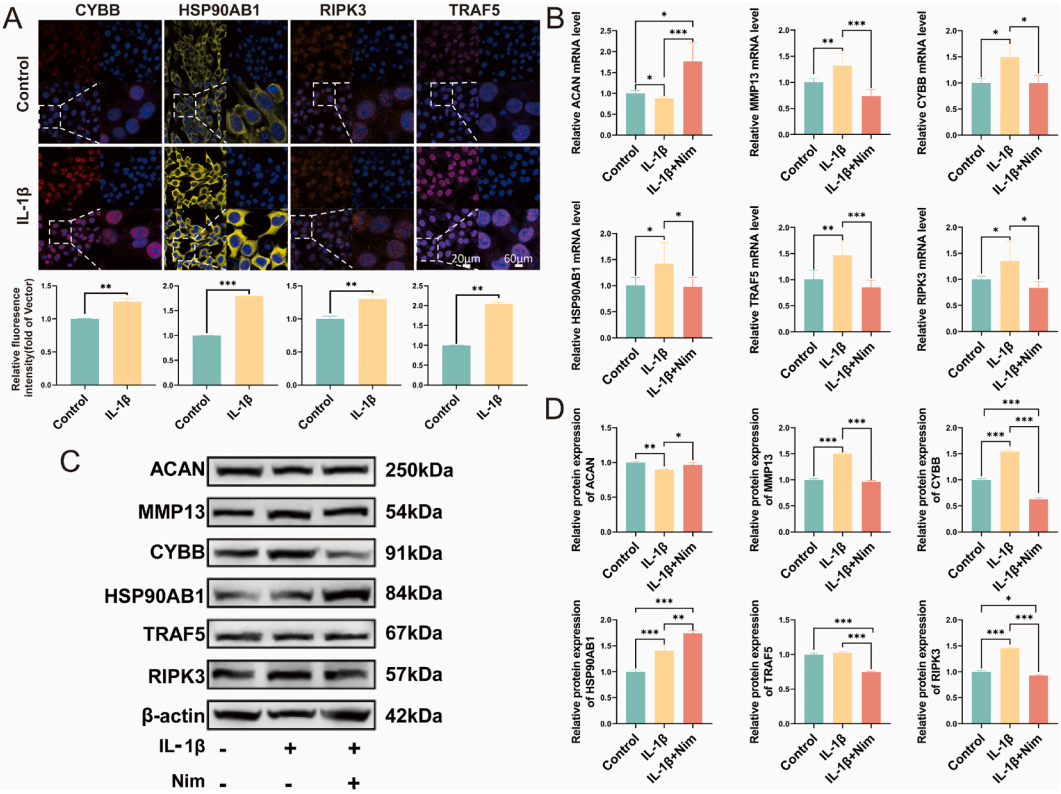

Fig. 4. Experimental validation of 4 hub genes expression. **A** Immunofluorescence images of the CYBB, HSP90AB1, CYBB and TRAF5 in the primary ADTC5 cells. Scale bar = 20 μm. **B** Differential expression of ACAN, MMP13 and 4 hub genes in control, OA, and nimesulide groups was verified by qRT-PCR (n = 3). **C, D** Western blotting and quantitative analysis of ACAN, MMP13, and 4 hub genes in control, OA, and nimesulide groups.

expression of ACAN was decreased. However, nimesulide was capable of reversing these changes, leading the OA-like ADTC5 cells to trend towards normality.

3.8. Necroptosis landscape in OA scRNA

To delve deeper into the diverse roles of necroptosis in chondrocytes, we utilized the GSE169454 dataset, comprising 3 control and 4 OA samples. Following thorough data cleaning, quality control, and batch effect removal, we obtained 58,540 cells (Fig. S3a). Using "Seurat" package for unsupervised clustering and dimensionality reduction, we identified 24 cell subpopulations (Fig. S3b). Referring to previously reported cellular marker genes [13,24,25], we finally annotated 7 major clusters including preFC, FC, RegC, HTC, EC, RepC, and HomC (Fig. 5A and B). OA group showed a significant increase in preFC, RegC, and HTC, and a decrease in HomC (Fig. 5C).

The top 20 genes of 7 clusters were shown in Fig. 5D. These genes clearly separated these cell types, and showed different GO enrichment results. FC subtype was mainly engaged in extracellular matrix (ECM) organization, RegC subtype was in positively regulating leukocyte migration, and HTC subtype in osteoblast differentiation. Fig. 5E and Fig. S3c revealed significant variations in necroptosis scores across chondrocyte subpopulations. Additionally, our findings indicated that necroptosis scores were elevated in FC and RegC compared to other subtypes (Fig. 5F). Moreover, we observed the expression of necrotic coregulated genes, including RIPK1, RIPK3, and MLKL, in all subtypes (Fig. S4a), and found that MLKL and RIPK1 were expressed in FC, RegC, and preFC subtypes.

3.9. Differences of necroptosis phenotypes in chondrocyte subpopulations

We divided the data into high and low scoring groups based on the median necroptosis score. Exploring the relationship between disease phenotypes and necroptosis scores, we performed KEGG enrichment analysis based on marker genes in different subgroups,

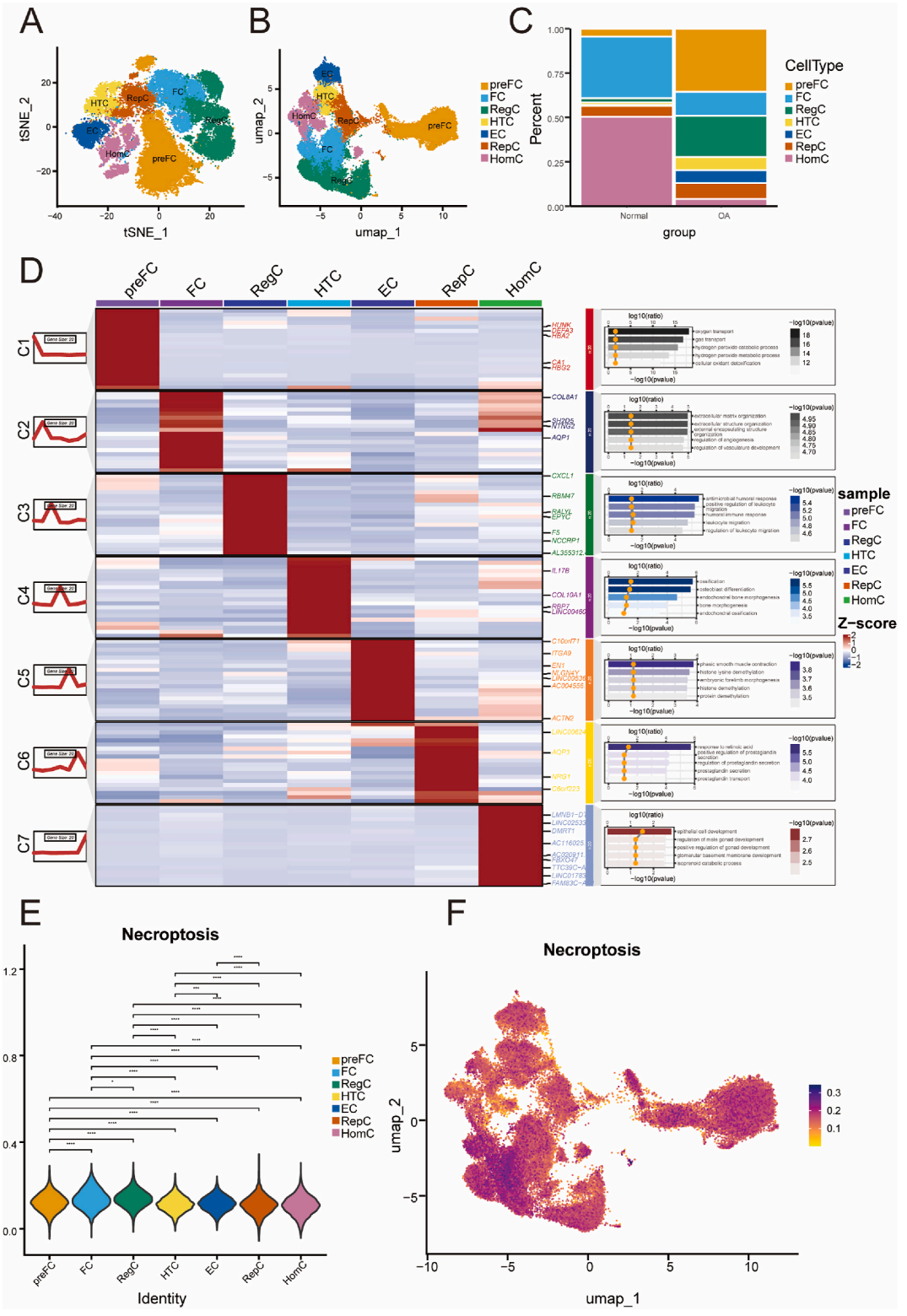

(caption on next page)

Fig. 5. Necroptosis microlandscape in OA single cell atlas. **A, B** Cells were clustered into 7 types via tSNE and UMAP dimensionality reduction algorithm, each color represented the annotated phenotype of each cluster. **C** Cell composition of control and OA groups. **D** Heatmap depicted the expression and GO enrichment analysis of the top 20 marker genes in the 7 cell clusters detected. **E** Violin plot showed the comprehensive score of 159 necroptosis-associated genes in all celltypes. **F** FeaturePlot_scCustom displayed the necroptosis composite score. (For interpretation of the references to color in this figure legend, the reader is referred to the Web version of this article.)

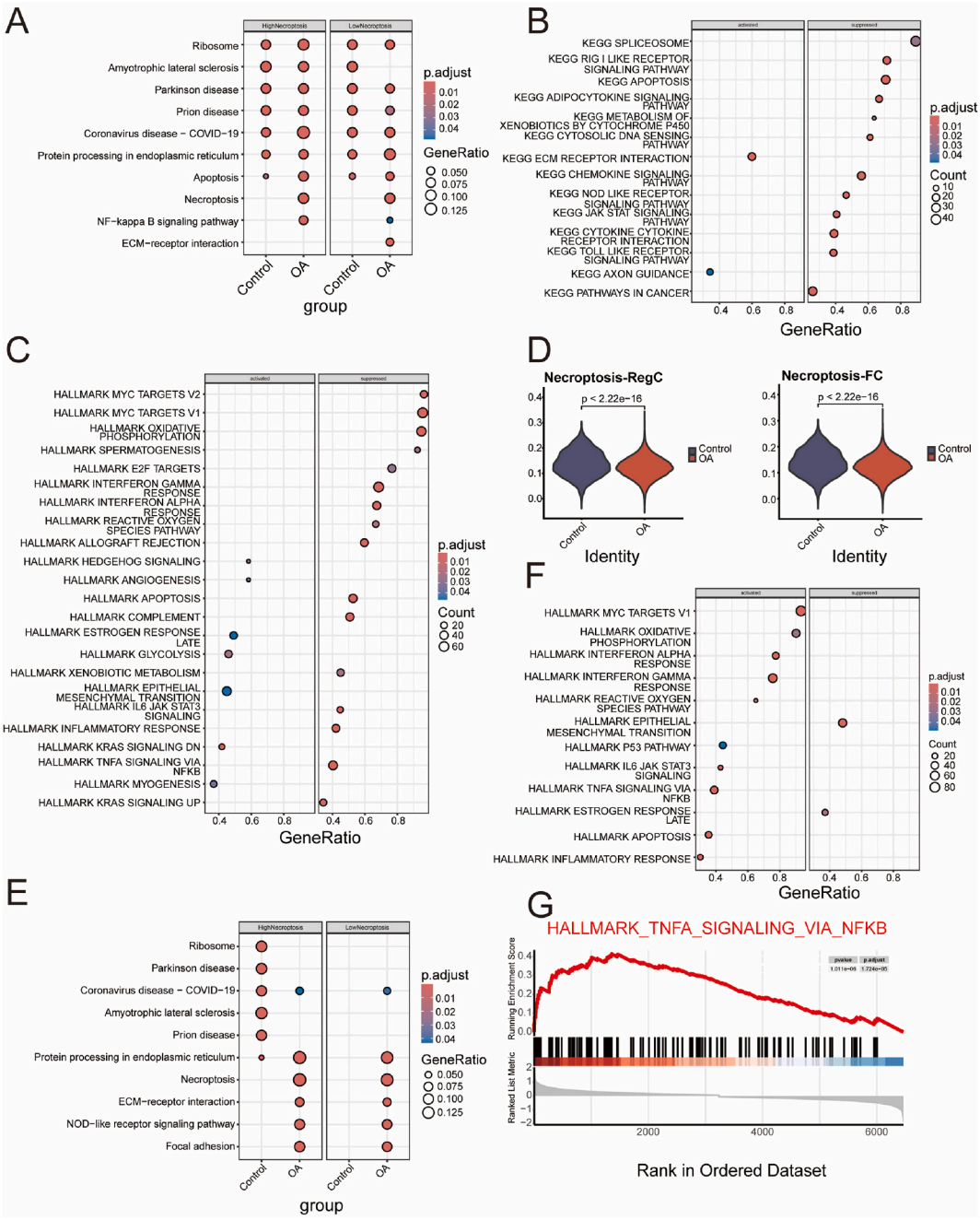

Fig. 6. Necroptosis landscape of different chondrocyte subtypes. **A** KEGG enrichment analysis of necroptosis scores. **B** GSEA analysis of KEGG pathways for necroptosis scores. **C** GSEA analysis of HALLMARK pathways for necroptosis scores. **D** Violin plot demonstrating the difference in necroptosis between RegC and FC. **E** KEGG enrichment analysis of necrosis score in RegC subtype. **F** GSEA analysis of HALLMARK pathways for necrosis score in RegC subtype. **G** gseaplot2 demonstrates TNF-α signaling via NF-κB pathways in RegC subtype.

and found that necroptosis pathway was focused in OA group, and the necroptosis pathway had a higher level of enrichment than the apoptotic pathway (Fig. 6A). GSEA analysis on the necroptosis phenotype revealed inhibition in both apoptotic and metabolism-related pathways. Notably, TNF-α signaling via NF-κB, essential for necroptosis initiation, was also inhibited (Fig. 6B and C).

Based on the expression of necroptosis in chondrocyte subtypes, we performed further functional enrichment analysis on RegC and FC subtypes. Initially, necroptosis phenotype was observed in RegC and FC subtypes (Fig. 6D). In RegC subtype, we observed a

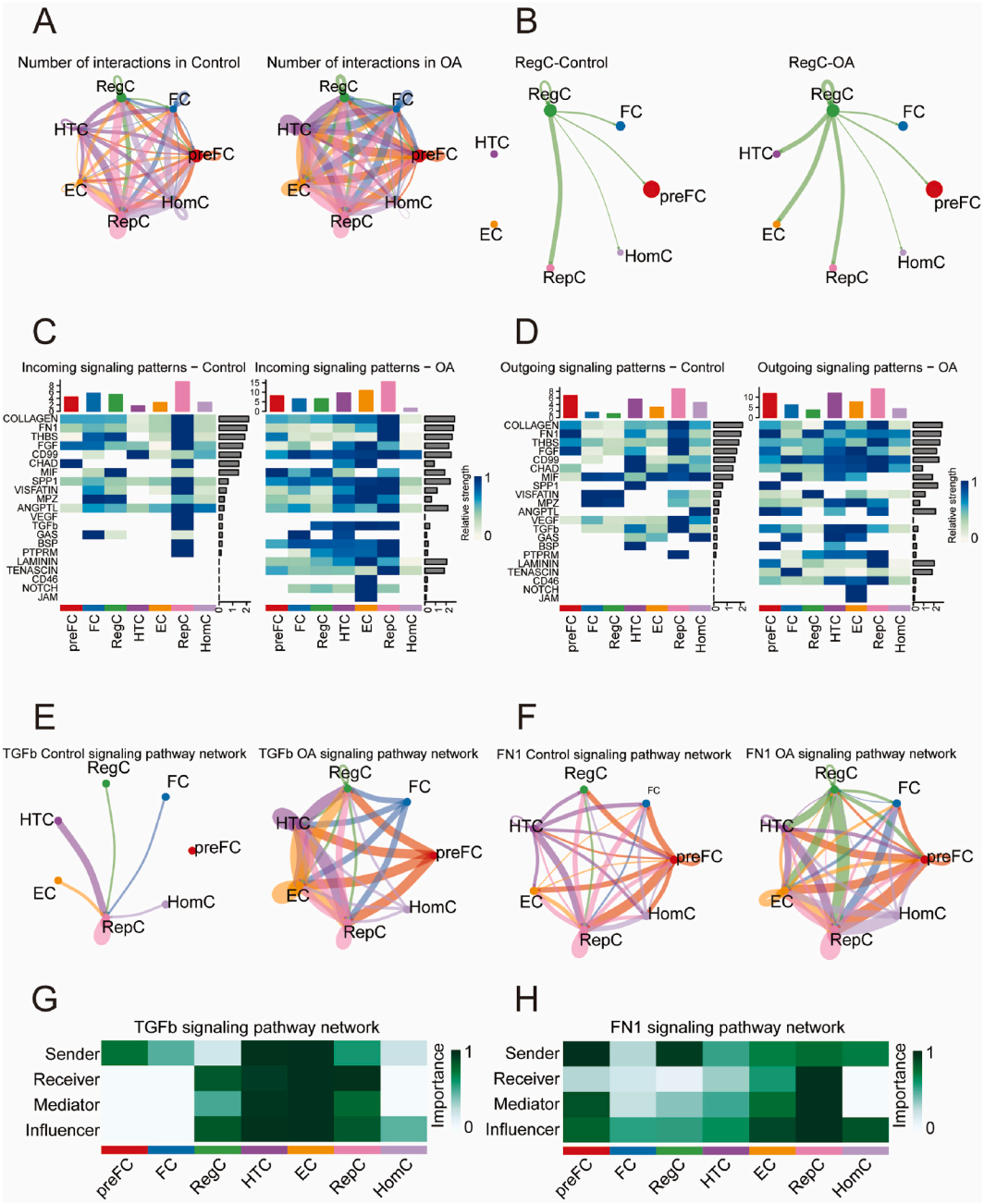

Fig. 7. CellChat analysis in scRNA-seq. **A** Circular plots of the number of cellular interactions between each chondrocyte subtype in control and OA groups. **B** Circular plots of the number of cellular interactions between RegC and other chondrocyte subpopulations in control and OA groups. **C, D** Heatmaps of the incoming (C) and outgoing (D) signaling pattern in each cell subtype mediated by individual signaling axes between control and OA groups. **E, F** Significant changes in cellular communication between RegC and other chondrocyte subpopulations in OA group compared to control samples. The circle plots showed the obvious changes in cell communication mediated by TGF-β (E) and FN1 (F) signaling pathways. **G, H** Heatmap showing the importance of four centrality indicators of the TGF-β signaling pathway (G) and the FN1 signaling pathway (H) in various cell subpopulations of OA group.

predominant enrichment of necroptosis, NOD-like receptor signaling, and ECM-receptor interaction pathways in OA group (Fig. 6E). GSEA analysis indicated activation of Toll-like receptor signaling, apoptosis, and TNF-α signaling via NF-κB pathways, alongside inhibition of the ECM-receptor interaction pathway (Fig. 6F, G, S4b). Conversely, GSEA analysis of FC subtype demonstrated activation of apoptosis, spliceosome, and MYC Targets V1 pathways (Figs. S4c, d, e). This suggested that while both RegC and FC subtypes underwent apoptosis, necroptosis also occurred in RegC subtype and might even dominate.

3.10. Communication differences between RegC and other chondrocyte subtypes

The summarized cell-cell communication network was shown in Fig. 7A, suggesting a significant change in the number of interactions between control and OA group. Our pathway enrichment results showed that RegC might be the main cell type for necroptosis in OA. Further, increased communication was also observed among RegC, HTC, and EC in OA group (Fig. 7B). To determine the signaling flow patterns in each chondrocyte subtype, changes in incoming and outgoing signaling patterns were compared in control and OA chondrocytes. CD99 signaling exhibited upregulation in both the incoming and outgoing groups. Whereas for RegC subtype, which is our concern, TGF-β signaling would be more afferent to RegC subtype in the OA group, but THBS signaling was less delivered to RegC subtype (Fig. 7C). In outgoing signaling within OA group, RegC subtype exhibited increased FN1 signaling, contrasted by a reduction in MIF signaling (Fig. 7D).

To further identify the changes of the above four signaling pathways, we demonstrated that the trend of signaling changes was consistent for RegC subtype, and we also found that preFC subtype in OA group had greater changes in TGF-β signaling (Fig. 7E, F, Figs. S5a and b) by means of network diagrams. Analysis of RegC subtype in OA group indicated that in TGF-β signaling, they were predominantly receivers and influencers (Fig. 7G). In FN1 signaling, RegC subtype was primarily senders, indicating that RegC affected other cells through FN1 signal exportation (Fig. 7H). In THBS signaling, RegC subtype primarily received signals from RegC subtype (Fig. S5c). In MIF signaling, RegC mainly acted as influencers and receivers, with predominant signals from FC subtype (Fig. S5d). This suggested that other chondrocyte subtypes influenced the onset of necroptosis in RegC subtype mainly through these 4 signaling pathways.

4. Discussion

Necroptosis has been shown to be involved in pathological cell death related to degenerative diseases, myocardial infarction, and autoimmune diseases [26–28]. In some of these diseases, necroptosis is often stimulated by TNF-α and the pan-aspartase inhibitor z-VAD-FMK [29]. However, in OA, studies have shown that inhibiting the key upstream molecule of TNF-α signaling, TNFR1-associated death domain protein (TRADD), can prevent the activation of RIPK1-TAK1-NF-κB signaling, thereby reducing necrosis in OA chondrocytes [30]. Simultaneously, it has been shown that DCC-2036 can directly inhibit RIPK1 and RIPK3 kinase activity, block chondrocyte necroptosis, and suppress inflammatory responses, thus protecting chondrocytes [31]. Although current research suggests a close association between necroptosis and the occurrence and progression of OA [32,33], the current efforts to alleviate OA necroptosis mainly focus on inhibiting RIPK1 and RIPK3 activity. Fortunately, advances in high-throughput sequencing technology and bioinformatics have enabled a deeper exploration of the molecular mechanisms of diseases, and the development of machine learning models has also aided in disease diagnosis [34,35]. Therefore, we performed a comprehensive analysis combining bulk RNA-seq and scRNA-seq data to construct a disease diagnostic model, searched for potential therapeutic agents for chondrocyte necroptosis, and targeted necroptosis-associated chondrocyte subtypes.

This study aimed to elucidate the mechanism of chondrocyte necroptosis by identifying necroptosis-related genes as diagnostic factors and therapeutic targets for OA. 4 key genes (RIPK3, CYBB, TRAF5, and HSP90AB1) were screened by differential gene analysis, WGCNA analysis and immune infiltration studies, and LASSO algorithm. RIPK3, as a key component of necrosomes, plays a crucial role in mediating inflammatory factors like TNFα, and orchestrating infection-induced necroptosis [36]. It has been shown that administration of necroptin-1 (Nec-1) significantly reduces the expression levels of RIPK1 and RIPK3 and inhibits programmed necrosis of osteoblasts, thereby reversing bone loss [37]. In our study, we found that RIPK3 was not only associated with other necroptosis-related genes, but also present in many of the enriched pathways. CYBB is the terminal component of a respiratory chain that transfers single electrons from cytoplasmic NADPH across the plasma membrane to molecular oxygen on the exterior. It encodes the β-chain of flavocytochrome b245 (also called as gp91phox or NOX2) and is a necessary component of the NADPH oxidase complex in phagocytes, such as granulocytes, monocytes, and macrophages [38]. Interestingly, CYBB and RIPK3 were both found in our study and seemed to exert special function in OA. In immune infiltration analysis, CYBB and RIPK3 were found to strongly correlate with macrophages, T cells and B cells. This might indicate that necrotic chondrocytes might accelerate the development of OA by activating immune cell infiltration and immune responses. TRAF5 is an adaptor protein that transduces intracellular signals from various TNF receptors, such as CD27 and CD40 [39]. TRAF5 has been screened as a diagnostic gene in colon adenocarcinoma, breast invasive carcinoma, and necroptosis studies in atherosclerosis [40–42]. HSP90AB1, also called HSP90beta, is a member of the heat shock protein 90 family which function as molecular chaperones [43]. The inhibition of HSP90beta has been shown to modulate NO and MMP-13 production in human OA chondrocytes [44].

The presence of necrosis in human and mouse cartilage degeneration was demonstrated by immunohistochemical analysis of the expression of necrosis markers RIP3, MLKL and p-MLKL [45]. However, the mechanism of necroptosis-related genes in the development of OA is not clear. To gain deeper insight at the cellular level, scRNA-seq analysis was performed. The results showed that the necroptosis score was significantly elevated in OA group, and focused on RegC, FC and preFC with performance differences. Necroptosis is triggered by death domain receptors and Toll-like receptor [46]. Meanwhile, in the pathway enrichment analysis combined

with bulk RNA seq and scRNA-seq, we found that necroptosis, TNF signaling pathway, NOD-like receptor signaling pathway, and Toll-like receptor signaling pathway were significantly enriched.

TNF-α is a pleiotropic inflammatory cytokine capable of inciting a survival, apoptotic, or necroptotic response based on the assembly of sequential but mutually exclusive cell death complexes [47,48], and current understanding of necroptosis revolves around the TNF-α receptor system. Some studies showed that the TNF signaling pathway was involved in the biological functions of DEGs related to necroptosis in lung adenocarcinoma, Stanford type A aortic dissection, and rheumatoid arthritis [49–51]. In addition, these cytokines mediate the activation of the NF-κB, a pathway that is known to disrupt chondrocyte homeostasis. More importantly, NF-κB signaling activation and TNF-α expression are positively correlated in necroptosis [52]. Increasing evidence proves that the innate immune system, specifically the Toll-like receptor (TLR), plays a key role in driving joint damage in OA and apoptosis is one of the key events in the TLR-induced innate immune response [53]. Meanwhile, activated NOD receptors stimulate the MAPK and NF-κB pathways via receptor interacting protein kinase 2 (RIPK2), predominantly eliciting inflammatory responses [54]. It has been shown that RegC subtype regulates multiple signaling pathways and interact with immune cells [55]. In addition, in the pathway enrichment analysis of RegC, we found that the Toll-like receptor, TNF-α signaling via NF-κB pathways, and NOD-like receptor pathways, which are closely related to necroptosis, were also activated. Interestingly, Dysregulated Toll-like receptor and NOD-like receptor pathways were identified in necroptosis studies in pulmonary hypertension, and RIPK3-mediated necroptosis may be associated with DAMP exposure and subsequent activation of TLR and NLR pathways [56]. Therefore, we hypothesized that necrosis-related genes might regulate necroptosis in RegC subtype by affecting these pathways.

In the molecular docking section, we targeted nimesulide through small molecule drug screening in the CTD database. Nimesulide is a relatively COX-2 selective, non-steroidal anti-inflammatory drug (NSAID) with analgesic and antipyretic properties [57]. Compared with celecoxib or rofecoxib, nimesulide shows better efficacy and faster onset of analgesia with a single dose in short-term trial [58]. However, research is still lacking on the modulation of OA progression by nimesulide through the regulation of chondrocyte necroptosis. We utilized an in vitro OA cell model and examined the effects of nimesulide on chondrocyte phenotype and necroptosis through RT-qPCR and Western blot. Our results confirmed that nimesulide might alleviate OA by reducing necroptosis in chondrocytes.

There are some limitations in the study, we utilized ATDC5 cells for nimesulide against the hub genes, and ATDC5 is a mouse-derived cell line, and further validation in human chondrocytes is needed. Whether interventions on necroptosis genes in animals or even humans can also ameliorate the occurrence of OA warrants further investigation.

5. Conclusions

In summary, we identified 4 significant necroptosis genes RIPK3, CYBB, TRAF5, and HSP90AB1 through a comprehensive multi-omics approach, and revealed the physiological functions of genes related to necroptosis in a specific chondrocyte subpopulation RegC. In addition, we found that the small molecule drug nimesulide could effectively decrease the expression of RIPK3 and CYBB. The results indicate that nimesulide could be used to treat OA by inhibiting chondrocyte necroptosis through down-regulation of RIK3 and CYBB genes.

Data availability

Data will be made available on request.

CRediT authorship contribution statement

Muhai Deng: Writing – original draft, Visualization, Validation, Methodology, Investigation, Formal analysis, Conceptualization. **Cong Tang:** Investigation. **Li Yin:** Visualization, Formal analysis. **Junjun Yang:** Writing – review & editing, Methodology, Investigation. **Zhiyu Chen:** Visualization, Validation, Methodology, Investigation. **Yunsheng Jiang:** Writing – review & editing, Methodology, Investigation. **Yang Huang:** Writing – review & editing, Visualization, Methodology, Investigation, Funding acquisition. **Cheng Chen:** Writing – review & editing, Writing – original draft, Supervision, Project administration, Funding acquisition, Conceptualization.

Declaration of competing interest

The authors declare that they have no known competing financial interests or personal relationships that could have appeared to influence the work reported in this paper.

Acknowledgements

This study was supported by Postdoctoral Research Project of Chongqing (2021XM3092), the Natural Science Foundation of Chongqing (cstb2022nscq-msx0139), and the Future Medical Innovation Team of Chongqing Medical University (W0080).

Appendix A. Supplementary data

Supplementary data to this article can be found online at https://doi.org/10.1016/j.heliyon.2024.e35263.

References

[1] F.E. Artuzi, R. Langie, M.C. Abreu, A.S. Quevedo, A. Corsetti, D. Ponzoni, et al., Rabbit model for osteoarthrosis of the temporomandibular joint as a basis for assessment of outcomes after intervention, Br. J. Oral Maxillofac. Surg. 54 (5) (2016) e33–e37.
[2] J. Stack, G.M. McCarthy, Cartilage calcification and osteoarthritis: a pathological association? Osteoarthritis Cartilage 28 (10) (2020) 1301–1302.
[3] Y. Jiang, R.S. Tuan, Origin and function of cartilage stem/progenitor cells in osteoarthritis, Nat. Rev. Rheumatol. 11 (4) (2015) 206–212.
[4] J.F. Xue, Z.M. Shi, J. Zou, X.L. Li, Inhibition of PI3K/AKT/mTOR signaling pathway promotes autophagy of articular chondrocytes and attenuates inflammatory response in rats with osteoarthritis, Biomed. Pharmacother. 89 (2017) 1252–1261.
[5] H. Yang, Y. Wen, M. Zhang, Q. Liu, H. Zhang, J. Zhang, et al., MTORC1 coordinates the autophagy and apoptosis signaling in articular chondrocytes in osteoarthritic temporomandibular joint, Autophagy 16 (2) (2020) 271–288.
[6] Z. Li, Z. Huang, H. Zhang, J. Lu, Y. Tian, Y. Wei, et al., P2X7 receptor induces pyroptotic inflammation and cartilage degradation in osteoarthritis via NF-κB/NLRP3 crosstalk, Oxid. Med. Cell. Longev. 2021 (2021) 8868361.
[7] M.Y. Ansari, K. Novak, T.M. Haqqi, ERK1/2-mediated activation of DRP1 regulates mitochondrial dynamics and apoptosis in chondrocytes, Osteoarthritis Cartilage 30 (2) (2022) 315–328.
[8] D.R. Park, J. Kim, G.M. Kim, H. Lee, M. Kim, D. Hwang, et al., Osteoclast-associated receptor blockade prevents articular cartilage destruction via chondrocyte apoptosis regulation, Nat. Commun. 11 (1) (2020) 4343.
[9] Q. Ran, H. Liang, M. Gu, W. Qi, C.A. Walter, L.J. Roberts 2nd, et al., Transgenic mice overexpressing glutathione peroxidase 4 are protected against oxidative stress-induced apoptosis, J. Biol. Chem. 279 (53) (2004) 55137–55146.
[10] J. Cheng, X. Duan, X. Fu, Y. Jiang, P. Yang, C. Cao, et al., RIP1 perturbation induces chondrocyte necroptosis and promotes osteoarthritis pathogenesis via targeting BMP7, Front. Cell Dev. Biol. 9 (2021) 638382.
[11] J. Jeon, H.J. Noh, H. Lee, H.H. Park, Y.J. Ha, S.H. Park, et al., TRIM24-RIP3 axis perturbation accelerates osteoarthritis pathogenesis, Ann. Rheum. Dis. 79 (12) (2020) 1635–1643.
[12] A. Linkermann, D.R. Green, Necroptosis, N. Engl. J. Med. 370 (5) (2014) 455–465.
[13] Q. Ji, Y. Zheng, G. Zhang, Y. Hu, X. Fan, Y. Hou, et al., Single-cell RNA-seq analysis reveals the progression of human osteoarthritis, Ann. Rheum. Dis. 78 (1) (2019) 100–110.
[14] Z. Lv, J. Han, J. Li, H. Guo, Y. Fei, Z. Sun, et al., Single cell RNA-seq analysis identifies ferroptotic chondrocyte cluster and reveals TRPV1 as an anti-ferroptotic target in osteoarthritis, EBioMedicine 84 (2022) 104258.
[15] K.M. Fisch, R. Gamini, O. Alvarez-Garcia, R. Akagi, M. Saito, Y. Muramatsu, et al., Identification of transcription factors responsible for dysregulated networks in human osteoarthritis cartilage by global gene expression analysis, Osteoarthritis Cartilage 26 (11) (2018) 1531–1538.
[16] R.H. Brophy, B. Zhang, L. Cai, R.W. Wright, L.J. Sandell, M.F. Rai, Transcriptome comparison of meniscus from patients with and without osteoarthritis, Osteoarthritis Cartilage 26 (3) (2018) 422–432.
[17] M.D. Aşık, S. Gürsoy, M. Akkaya, L.D. Kozacı, M. Doğan, M. Bozkurt, Microarray analysis of cartilage: comparison between damaged and non-weight-bearing healthy cartilage, Connect. Tissue Res. 61 (5) (2020) 456–464.
[18] U. Sarkans, M. Gostev, A. Athar, E. Behrangi, O. Melnichuk, A. Ali, et al., The BioStudies database-one stop shop for all data supporting a life sciences study, Nucleic Acids Res. 46 (D1) (2018) D1266–d1270.
[19] W. Fu, A. Hettinghouse, Y. Chen, W. Hu, X. Ding, M. Chen, et al., 14-3-3 epsilon is an intracellular component of TNFR2 receptor complex and its activation protects against osteoarthritis, Ann. Rheum. Dis. 80 (12) (2021) 1615–1627.
[20] C. von Mering, M. Huynen, D. Jaeggi, S. Schmidt, P. Bork, B. Snel, STRING: a database of predicted functional associations between proteins, Nucleic Acids Res. 31 (1) (2003) 258–261.
[21] A.P. Davis, T.C. Wiegers, R.J. Johnson, D. Sciaky, J. Wiegers, C.J. Mattingly, Comparative Toxicogenomics database (CTD): update 2023, Nucleic Acids Res. 51 (D1) (2023) D1257–d1262.
[22] S. Kim, J. Chen, T. Cheng, A. Gindulyte, J. He, S. He, et al., PubChem 2023 update, Nucleic Acids Res. 51 (D1) (2023) D1373–d1380.
[23] S. Jo, T. Kim, V.G. Iyer, W. Im, CHARMM-GUI: a web-based graphical user interface for CHARMM, J. Comput. Chem. 29 (11) (2008) 1859–1865.
[24] C.H. Chou, V. Jain, J. Gibson, D.E. Attarian, C.A. Haraden, C.B. Yohn, et al., Synovial cell cross-talk with cartilage plays a major role in the pathogenesis of osteoarthritis, Sci. Rep. 10 (1) (2020) 10868.
[25] I. Korsunsky, N. Millard, J. Fan, K. Slowikowski, F. Zhang, K. Wei, et al., Fast, sensitive and accurate integration of single-cell data with Harmony, Nat. Methods 16 (12) (2019) 1289–1296.
[26] M. Luedde, M. Lutz, N. Carter, J. Sosna, C. Jacoby, M. Vucur, et al., RIP3, a kinase promoting necroptotic cell death, mediates adverse remodelling after myocardial infarction, Cardiovasc. Res. 103 (2) (2014) 206–216.
[27] K. Newton, D.L. Dugger, A. Maltzman, J.M. Greve, M. Hedehus, B. Martin-McNulty, et al., RIPK3 deficiency or catalytically inactive RIPK1 provides greater benefit than MLKL deficiency in mouse models of inflammation and tissue injury, Cell Death Differ. 23 (9) (2016) 1565–1576.
[28] S.H. Yang, D.K. Lee, J. Shin, S. Lee, S. Baek, J. Kim, et al., Nec-1 alleviates cognitive impairment with reduction of Aβ and tau abnormalities in APP/PS1 mice, EMBO Mol. Med. 9 (1) (2017) 61–77.
[29] M. Ogasawara, T. Yano, M. Tanno, K. Abe, S. Ishikawa, T. Miki, et al., Suppression of autophagic flux contributes to cardiomyocyte death by activation of necroptotic pathways, J. Mol. Cell. Cardiol. 108 (2017) 203–213.
[30] K. Sun, Z. Guo, J. Zhang, L. Hou, S. Liang, F. Lu, et al., Inhibition of TRADD ameliorates chondrocyte necroptosis and osteoarthritis by blocking RIPK1-TAK1 pathway and restoring autophagy, Cell Death Dis. 9 (1) (2023) 109.
[31] L. Piao, D. Wu, C. Rui, Y. Yang, S. Liu, J. Liu, et al., The Bcr-Abl inhibitor DCC-2036 inhibits necroptosis and ameliorates osteoarthritis by targeting RIPK1 and RIPK3 kinases, Biomed. Pharmacother. 161 (2023) 114528.
[32] Y. Gong, J. Qiu, J. Ye, T. Jiang, W. Zhang, X. Zheng, et al., AZ-628 delays osteoarthritis progression via inhibiting the TNF-α-induced chondrocyte necroptosis and regulating osteoclast formation, Int. Immunopharm. 111 (2022) 109085.
[33] Y. Zhou, S. Lin, Z. Huang, C. Zhang, H. Wang, B. Li, et al., Receptor-interacting protein 1 inhibition prevents mechanical stress-induced temporomandibular joint osteoarthritis by regulating apoptosis and later-stage necroptosis of chondrocytes, Arch. Oral Biol. 147 (2023) 105612.
[34] Y. Zhang, N. Imirzian, C. Kurze, H. Zheng, D.P. Hughes, D.Z. Chen, Learning from algorithm-generated pseudo-annotations for detecting ants in videos, Sci. Rep. 13 (1) (2023) 11566.
[35] Y. Zhang, L. Zhang, S. Cao, Y. Wang, X. Ling, Y. Zhou, et al., A nomogram model for predicting the risk of checkpoint inhibitor-related pneumonitis for patients with advanced non-small-cell lung cancer, Cancer Med. 12 (15) (2023) 15998–16010.
[36] S. Liu, K. Joshi, M.F. Denning, J. Zhang, RIPK3 signaling and its role in the pathogenesis of cancers, Cell. Mol. Life Sci. 78 (23) (2021) 7199–7217.
[37] H. Cui, Y. Zhu, Q. Yang, W. Zhao, S. Zhang, A. Zhou, et al., Necrostatin-1 treatment inhibits osteocyte necroptosis and trabecular deterioration in ovariectomized rats, Sci. Rep. 6 (2016) 33803.

[38] A. Heydari, F. Abolnezhadian, M. Sadeghi-Shabestari, A. Saberi, A. Shamsizadeh, A.A. Ghadiri, et al., Identification of Cytochrome b-245, beta-chain gene mutations, and clinical presentations in Iranian patients with X-linked chronic granulomatous disease, J. Clin. Lab. Anal. 35 (2) (2021) e23637.
[39] T. So, H. Nagashima, N. Ishii, TNF receptor-associated factor (TRAF) signaling network in CD4(+) T-lymphocytes, Tohoku J. Exp. Med. 236 (2) (2015) 139–154.
[40] Z. Peng, K. Wang, S. Wang, R. Wu, C. Yao, Identification of necroptosis-related gene TRAF5 as potential target of diagnosing atherosclerosis and assessing its stability, BMC Med. Genom. 16 (1) (2023) 139.
[41] Q. Zhou, Y. Xu, L. Shen, X. Yang, L. Wang, Identification of a novel necroptosis-related classifier to predict prognosis and guide immunotherapy in breast invasive carcinoma, Front. Oncol. 12 (2022) 852365.
[42] H. Lan, Y. Liu, J. Liu, X. Wang, Z. Guan, J. Du, et al., Tumor-associated macrophages promote oxaliplatin resistance via METTL3-mediated m(6)A of TRAF5 and necroptosis in colorectal cancer, Mol. Pharm. 18 (3) (2021) 1026–1037.
[43] M. Haase, G. Fitze, HSP90AB1: helping the good and the bad, Gene 575 (2 Pt 1) (2016) 171–186.
[44] V. Calamia, M.C. de Andrés, N. Oreiro, C. Ruiz-Romero, F.J. Blanco, Hsp90β inhibition modulates nitric oxide production and nitric oxide-induced apoptosis in human chondrocytes, BMC Muscoskel. Disord. 12 (2011) 237.
[45] J. Riegger, R.E. Brenner, Evidence of necroptosis in osteoarthritic disease: investigation of blunt mechanical impact as possible trigger in regulated necrosis, Cell Death Dis. 10 (10) (2019) 683.
[46] D. Bertheloot, E. Latz, B.S. Franklin, Necroptosis, pyroptosis and apoptosis: an intricate game of cell death, Cell. Mol. Immunol. 18 (5) (2021) 1106–1121.
[47] K. Moriwaki, F.K. Chan, RIP3: a molecular switch for necrosis and inflammation, Genes Dev. 27 (15) (2013) 1640–1649.
[48] P. Mandal, S.B. Berger, S. Pillay, K. Moriwaki, C. Huang, H. Guo, et al., RIP3 induces apoptosis independent of pronecrotic kinase activity, Mol Cell 56 (4) (2014) 481–495.
[49] Q. He, H. Ding, Bioinformatics analysis of rheumatoid arthritis tissues identifies genes and potential drugs that are expressed specifically, Sci. Rep. 13 (1) (2023) 4508.
[50] K. Lei, B. Tan, R. Liang, Y. Lyu, K. Wang, W. Wang, et al., Development and clinical validation of a necroptosis-related gene signature for prediction of prognosis and tumor immunity in lung adenocarcinoma, Am. J. Cancer Res. 12 (11) (2022) 5160–5182.
[51] F. Liu, T. Wei, L. Liu, F. Hou, C. Xu, H. Guo, et al., Role of necroptosis and immune infiltration in human Stanford type A aortic dissection: novel insights from bioinformatics analyses, Oxid. Med. Cell. Longev. 2022 (2022) 6184802.
[52] D. Wallach, T.B. Kang, A. Kovalenko, Concepts of tissue injury and cell death in inflammation: a historical perspective, Nat. Rev. Immunol. 14 (1) (2014) 51–59.
[53] G. Barreto, M. Manninen, K.E. K, Osteoarthritis and toll-like receptors: when innate immunity meets chondrocyte apoptosis, Biology 9 (4) (2020).
[54] M.J. Jurynec, C.M. Gavile, M. Honeggar, Y. Ma, S.R. Veerabhadraiah, K.A. Novak, et al., NOD/RIPK2 signalling pathway contributes to osteoarthritis susceptibility, Ann. Rheum. Dis. 81 (10) (2022) 1465–1473.
[55] Y. Gu, Y. Hu, H. Zhang, S. Wang, K. Xu, J. Su, Single-cell RNA sequencing in osteoarthritis, Cell Prolif. 56 (12) (2023) e13517.
[56] G. Xiao, W. Zhuang, T. Wang, G. Lian, L. Luo, C. Ye, et al., Transcriptomic analysis identifies Toll-like and Nod-like pathways and necroptosis in pulmonary arterial hypertension, J. Cell Mol. Med. 24 (19) (2020) 11409–11421.
[57] A. Bennett, G. Villa, Nimesulide: an NSAID that preferentially inhibits COX-2, and has various unique pharmacological activities, Expet Opin. Pharmacother. 1 (2) (2000) 277–286.
[58] M. Bianchi, M. Broggini, A randomised, double-blind, clinical trial comparing the efficacy of nimesulide, celecoxib and rofecoxib in osteoarthritis of the knee, Drugs 63 (Suppl 1) (2003) 37–46.